Volume 1 | Number 1 | Jan 2013 | Pages 1–100

Analyst

www.rsc.org/analyst

ROYAL SOCIETY OF CHEMISTRY

www.rsc.org/analyst

An Attenuated Total Reflection (ATR) and Raman spectroscopic investigation into the effects of chloroquine on *Plasmodium falciparum*-infected red blood cells

M. Kozicki[1], D. J. Creek[2], A. Sexton[2], B. J. Morahan[4], A. Wesełucha-Birczyńska[1] and B. R. Wood[3]*

[1] Faculty of Chemistry, Ingardena 3, Kraków, Poland

[2] Monash Institute of Pharmaceutical Sciences, Monash University, Parkville, VIC 3052, Australia

[3]Centre for Biospectroscopy and School of Chemistry, Monash University, Wellington Rd., VIC. 3800, Australia

[4]Department of Microbiology, Monash University, Clayton, VIC 3800, Australia

*e-mail: bayden.wood@monash.edu

Abstract

Attenuated Total Reflection Fourier Transform Infrared (ATR-FTIR) and Raman spectroscopy were used to compare chloroquine (CQ)-treated and untreated cultured *Plasmodium falciparum*-infected human red blood cells (iRBCs). The studies were carried out in parallel from the same starting cultures using both spectroscopic techniques, in duplicate. ATR FTIR spectra showed modifications in the heme vibrational bands as well as increases in the CH_2/CH_3 stretching bands in the 3100 -2800 cm^{-1} region of CQ-treated iRBCs consistent with an increase in lipid content. Other changes consisted of secondary structural variations including shifts in the amide I and II modes, along with changes in RNA and carbohydrate bands. Raman microspectroscopy of single red blood cells using 532 nm revealed subtle changes in the positions and intensity of ν_{37} of the core size region marker band and ν_4 in the pyrrole ring-stretching region between untreated and CQ-treated iRBCs. Similar patterns in the corresponding relations were also observed in the non-fundamental (overtone region) between the control and treated cells. These differences were consistent with higher levels of oxygenated hemoglobin (oxyHb) in the treated cells as shown in a Principle Component Analysis (PCA) loadings plot. The results obtained demonstrate that vibrational spectroscopic techniques can provide insight into the effect of quinolines on iRBCs and thus may assist understanding the sensitivity and resistance of new and existing anti-malarial drugs.

1. Introduction

Plasmodium falciparum (P. falciparum) causes the most severe form of human malaria. Quinoline-containing antimalarial drugs like chloroquine (CQ) are commonly used for the treatment of *P. falciparum* because they are safe and low-cost [1]. However, drug resistance is common in Asia and Africa, restricting the effective use of CQ to a few countries in the Caribbean and Central America. In these countries WHO recommends a combination of chloroquine and artemisinin for all *P. falciparum* confirmed cases [2]. In malaria-endemic countries where CQ resistance is prevalent, artemisinin combination therapies containing other quinoline antimalarials are recommended as first-line treatment for malaria. An improved understanding of the effect of quinoline antimalarials on infected red blood cells is important for the optimal utilization of antimalarial medicines and the development of new antimalarial combinations.

The antimalarial mechanism of CQ action is still not fully understood. Published theories include DNA binding and the inhibition of various enzymes and transporter molecules [3]. The most accepted theory is that CQ interferes with hemoglobin digestion by the *P. falciparum* parasite in the digestive vacuole (DV) [4]. During digestion, the protein moiety is catabolized and the heme is detoxified by polymerisation to form hemozoin. CQ accumulates in the acidic vacuole where it becomes ionised (to CQ^{2+}) resulting in membrane impermeability to the charged forms of the drug [5]. Chloroquine binds to ferriprotoporphyrin IX (FPIX) to form the FPIX - CQ complex, which disrupts membrane function and is involved in parasite cell auto-digestion [6]. The mechanism of CQ resistance is by decreased accumulation of chloroquine in the DV, conferred by mutations in the chloroquine resistance transporter (*Pf*CRT) [7]. Quinoline based drugs are thought to bind with FPIX via π-π interactions, which could in theory reduce the excitonic effects in the porphyrin array resulting in a reduction in the intensity of vibrational modes sensitive to the electron density of the porphyrin rings [8]. In this study we apply Raman and FTIR-ATR spectroscopy to monitor the interactions between chloroquine and iRBCs. These methods have enabled us to detect the effect of CQ on the cellular biochemistry of iRBCs providing information about molecular changes that occur to iRBCs in response to CQ therapy.

2. Experimental

2.1 *Plasmodium falciparum* culture

The 3D7 strain of *P. falciparum* was maintained in human red blood cells (RBCs) suspended in complete RPMI media (RPMI 1640 [10.4 g/L], HEPES [5.94 g/L], hypoxanthine [5 mg/L], Albumax II [5 g/L] and $NaHCO_3$ [2.14 g/L]), as previously described [9]. Trophozoite-stage *P. falciparum*-infected RBCs (iRBCs) were purified by magnetic sorting, as per the manufacturer's instructions (VarioMACS, Miltenyi Biotech). Purified iRBCs were incubated with or without 1 μM CQ for 5 hours at 37 ºC under a gas environment of 92% N_2, 5% CO_2 and 1% O_2. The iRBCs were then washed in ice-cold normal saline to quench metabolism, and kept on ice before being used for spectroscopic measurements. The experiment was performed in duplicate on separate occasions using different cultures with red blood cells from different donors.

2.2 Preparation of blood samples

CQ-treated and untreated iRBCs suspended in normal saline (~10^9 cells/mL) were used to perform ATR and Raman measurements simultaneously. In the case of Raman 30 different cells were measured, while for ATR 30 random sub-populations of cells were analysed. Measurements on iRBCs were repeated two times in order to ensure reproducibility of each trial and they were also randomized.

Samples for Raman measurements were placed on gold-coated Petri dishes. The gold coating was prepared using a Quorum Q150T S sputter coater. Metal-coated Petri dishes make good substrates for Raman measurements because they have high reflectivity and they are not Raman active. Poly-L-lysine (0.01% solution, Sigma-Aldrich) was applied to the gold-coated Petri dishes and then dried with a hair dryer. The Petri dish was then filled to ¾ of the total volume of the dish with phosphate buffered saline (PBS, pH= 7.4, Sigma-Aldrich) and 5 μL iRBCs were added. The Petri dish was left for 10 mins to allow the iRBCs to settle to the bottom and adhere to the poly-L-lysine.

Samples for ATR-FTIR spectroscopy were prepared in an aliquot of approximately 30 μl of iRBCs suspension, placed on the silicon window and rapidly dried with a blow dryer. For each sample, 4 replicate spectra were recorded in order to ensure precision and reproducibility of each sample.

Air-drying of red blood cells results in the formation of a mixture of hemichrome and oxyhemoglobin [10]. After prolonged atmospheric exposure methemoglobin can form but this is avoided with a short drying time. While such changes are observable in Raman spectra of air-dried cells the effect would be negligible in the case of ATR-FTIR spectra where only gross changes in protein, lipid, nucleic acids and carbohydrates are observed and not subtle perturbation of the heme group.

2.3 Chloroquine sample

A drop of 1mM CQ in DMSO was dried onto an aluminium-coated slide. The Raman spectrum was collected using 532 nm excitation wavelength with 0.5 mW power at the sample (Fig. 7). The same CQ solution was dried on a silicon window of the ATR accessory and FTIR spectrum was collected (Fig. 1).

2.4 Instrumentation

2.4.1 Raman microspectroscopy

The Raman spectra of blood samples, in the range of 3700– 100 cm^{-1}, were collected using a confocal Raman WITec alpha300 R microspectrometer (WITec GmbH, Germany) with a CCD camera cooled to –60 ºC. Measurements were performed using 532 nm laser and 0.1 mW power with a 60x water immersion objective. The WITec system was controlled using WITec Project 2.10 software.

2.4.2 ATR-FTIR spectroscopy

ATR-FTIR measurements, in the range of 4000 – 600 cm^{-1}, were recorded using a BioATRCell II FT-IR-Accessory (Bruker Optic, Ettingen, Germany) coupled to a Bruker IFS Equinox FTIR system. The FT-IR spectrometer was fitted with a N_2-cooled MCT (mercury−cadmium−telluride) detector. For each spectrum 50 interferograms were co–added. The Bruker system was controlled using OPUS v. 6.0 software.

2.5 Data analysis

2.5.1 ATR-FTIR data analysis

OPUS software (Bruker Optic) was applied to pre-process the spectral data. ATR data, raw spectra, were vector-normalized and the second derivative calculated. PCA was performed with Unscrambler X software packages (v. 10.0.1, Camo Software, Oslo, Norway) on second derivatives in the chosen spectral regions. Each point, in the PCA scores plot, represents average spectra consisting of 4 replicates for each sample.

2.5.2 Raman spectra analysis

The Raman spectra were smoothed using a Savitzky−Golay smoothing algorithm (six smoothing points), baseline corrected and unit vector normalised. A K-means Cluster Analysis (KCA) classification model was used to predict a sample's class based on its closest neighbors and random spectra selected from the major classes for PCA using Unscrambler X software packages (v. 10.0.1, Camo Software, Oslo, Norway).

The PCA model was built based on average spectra recorded from the hemoglobin part of each cell for the two groups (untreated and CQ-treated) each comprising of 30 different iRBCs. The PCA scores plots shows a clear separation based on differences in the amount of hemoglobin between the clusters (Fig. 10). There were no significant differences in the spectra recorded of hemozoin within the cells.

3. Results and discussion

ATR-FTIR and Raman spectra were acquired from CQ-treated and untreated iRBCs. ATR-FTIR is very sensitive to the lipid moieties, proteins, RNA/DNA and carbohydrate vibrations while Raman spectroscopy is sensitive to highly symmetric and chromophoric molecules like the heme group form hemoglobin and hemozoin and provides information on the heme core size marker bands, pyrrole ring stretching modes and C-H modes from the porphyrin..

3.1 ATR-FTIR spectroscopy
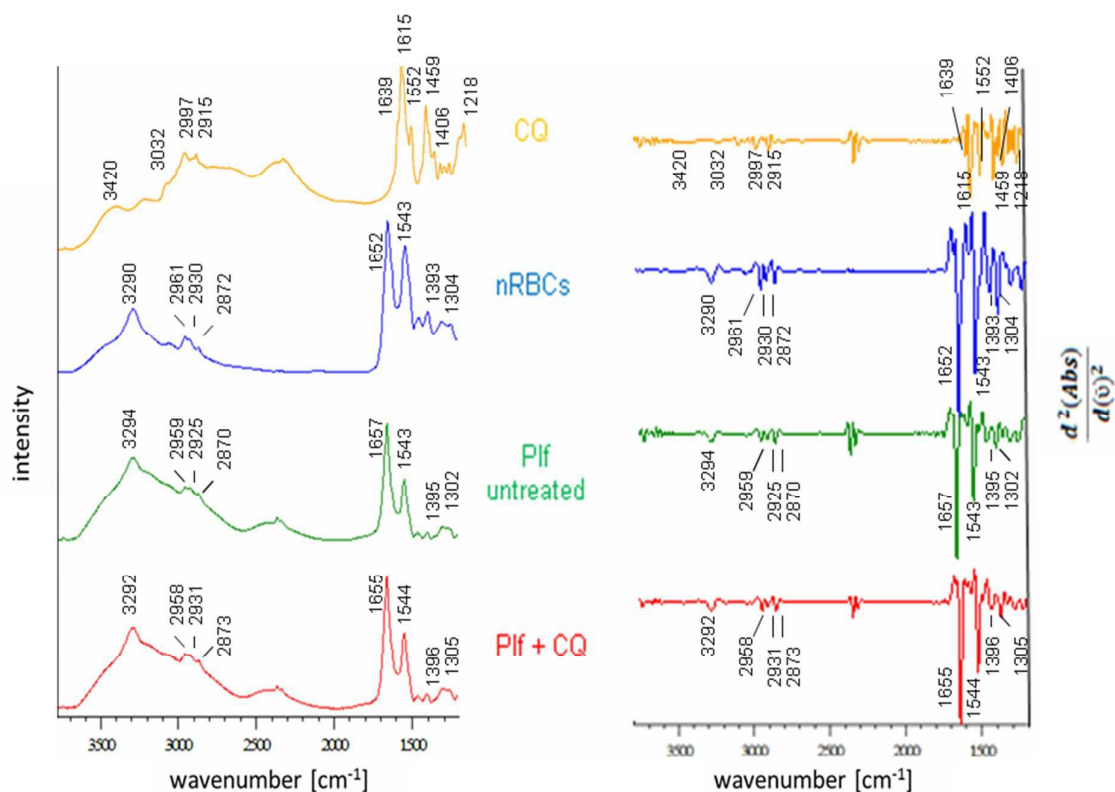
Figure 1 ATR-FT-IR and their corresponding 2nd derivative spectra in the 3800 -1200 cm^{-1} spectral range for chloroquine (CQ), non-infected red blood cells (nRBCs), untreated (Plf untreated) and CQ-treated (Plf+CQ) *P. falciparum* iRBCs.

Table 1. Observed wavenumber values and their assignments for non-infected red blood cells (nRBCs), untreated (Plf) and chloroquine-treated (Plf+CQ) *P. falciparum* - iRBCs.

ATR band positions [cm^{-1}]			Assignments [11, 12]
nRBC	Plf	Plf + CQ	
3290	3294	3292	O-H sym. str.
2961	2959	2958	CH$_3$ asym. str.
2930	2925	2931	CH$_2$ asym. str.
2872	2870	2873	CH$_2$ asym. str.
1652	1657	1655	amide I; CN str.; NH bend
1543	1543	1544	amide II; NH bend; CN str.
1393	1395	1396	N-CH$_3$ sym. def.; ν (COO$^-$);
1304	1302	1305	amide III; CN str.; NH bend

Table 2. ATR bands positions and their assignments for chloroquine

ATR band positions [cm^{-1}]	Assignments [12, 13]
3420	O-H asym. str.
3032	C-H str.
2997	
2915	
1639	ν (CC/CN)
1618	ν (CC/CN)
1552	
1464	ν (CC/CN), δ (CCC/NCC)
1406	
1218	ν (CC); δ (CH)

ATR-FT-IR spectra for nRBCs and iRBCs (Fig. 1, Tab. 1) show amide I, amide II, COO$^-$ from carboxylate groups of proteins and CH_2/CH_3 deformations from lipids. In addition, there are vibrations in the 3500-3100 cm^{-1} region derived from the water O-H asymmetric and symmetric stretching vibrations. Prominent bands in the CQ spectrum (Fig. 1, Tab. 2) are assigned to ν(CC) and ν(CN) quinoline vibrations.

Multiplicative effects can dominate spectral data of heterogenous samples. In such cases second derivatives can decrease baseline offset and also reduce quadratic baseline effects caused by particle scatter. For multivariate analysis the second derivative of FTIR-ATR spectra were used. When interpreting these spectra, the loadings maxima become minima in the corresponding scores plot.
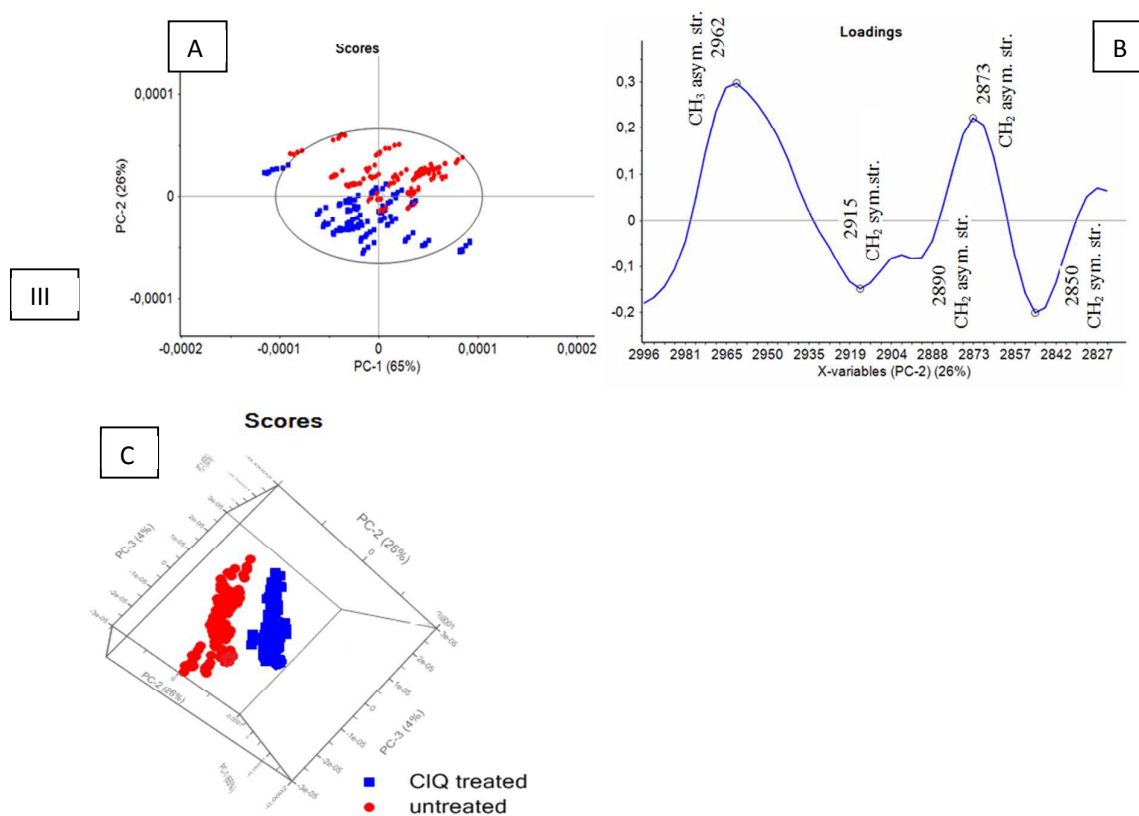
Fig. 2 PCA applied to second derivative ATR-FTIR in the spectral range 3000 - 2800 cm^{-1} A) PC-1 and PC-2 scores plot along of untreated (red dots) and CQ-treated (blue dots) *P. falciparum* - iRBCs data sets. B) PC-2 loadings plot showing the C-H stretching region (3000 - 2800 cm^{-1}). C) 3D scores plot for PC-1 vs. PC-2 vs. PC-3.

The C-H stretching region shows a good separation for the untreated and CQ-treated cells in the PC1 vs. PC2 (vs. PC3 for 3D) scores plot. Bands at 2850, 2873, 2890, 2915 and 2962 cm^{-1} are assigned to the symmetric and asymmetric C-H stretching vibrations of methyl and methylene groups, which originate from saturated lipids in the CQ infected cells. This may result from the insertion of *P. falciparum*-derived lipids into the RBC plasma membrane and/or a change in lipid distribution from RBC membranes into DVs [14]. Upon infection of RBCs *P. falciparum* modifies the RBC plasma membrane by increasing its rigidity, changing the lipid composition and distribution of the phospholipids in the bilayer resulting in an increase in permeability [15]. Minima bands in the loadings plot (Fig. 2B) at wavenumber values of 2915 and 2890 cm^{-1} are assigned to vibrations of the CH_2 groups adjacent to the carboxyl residue and methyne (H–C=C-) bond. The band at 2850 cm^{-1} is assigned to the symmetric CH_2 vibration and is indicative unsaturated lipids [16].
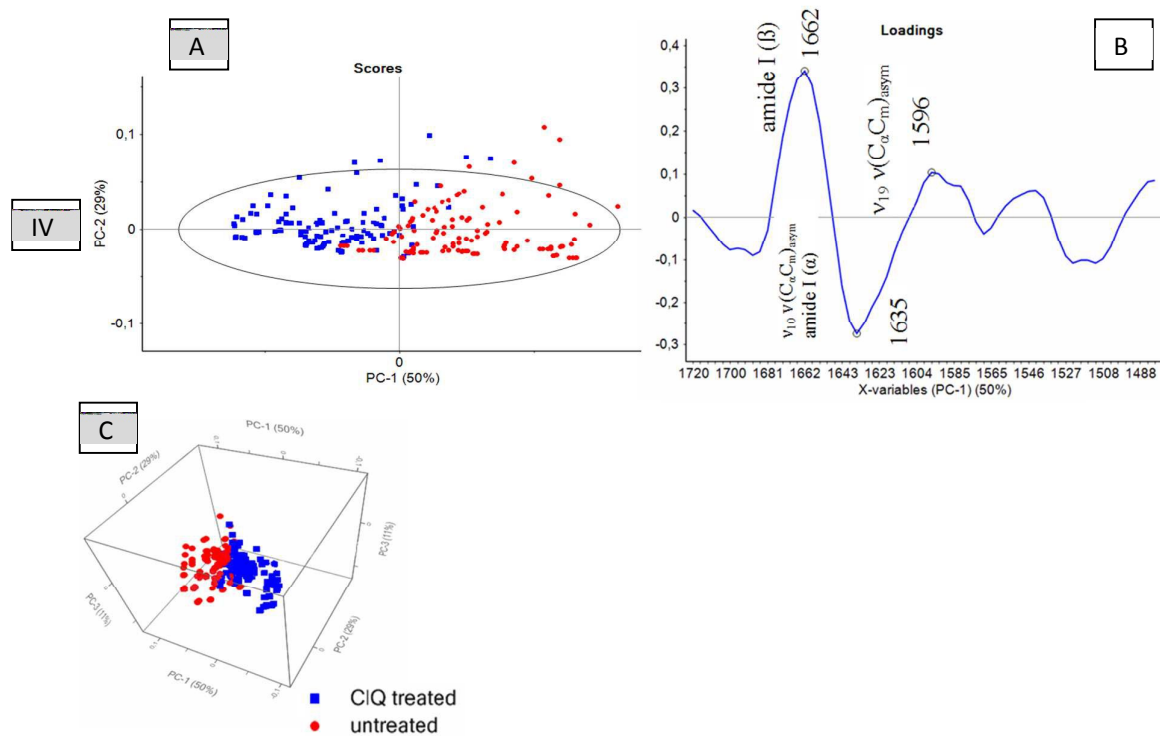
Fig. 3 The results of PCA applied to second derivative ATR-FTIR spectra of untreated (red dots) and CQ-treated (blue dots) *P. falciparum* - iRBCs in the spectral range 1720 - 1500 cm^{-1} showing A) scores for PC-1 and PC-2 B) loadings for PC-1 and C) a three–dimensional scores plot for PC-1 vs PC-2 vs PC-3.

The shifts observed in the protein modes at 1662 and 1635 cm^{-1} in the loadings plot for the 1720-1480 cm^{-1} range are possibly indicative of a difference in protein secondary structure between the two experimental groups (Fig. 3). The β-conformation of the hemoglobin molecule appears at 1662 cm^{-1} in the CQ-treated iRBCs and at 1635 cm^{-1} for the untreated iRBCs indicative of a higher concentration of α-helical in the latter. Remembering that because we are looking at the second derivative the positive scores are associated with the negative loadings and vice versa. The dramatic conformational changes are related to the degradation of hemoglobin, which is first converted into α-hematin (ferriprotoporphyrin IX) and ultimately to β-hematin. The binding of CQ to α-hematin prevents the free heme becoming incorporated into the hemozoin crystal and hence the free α-hematin can disrupt cell membranes and inhibit enzymes.

9
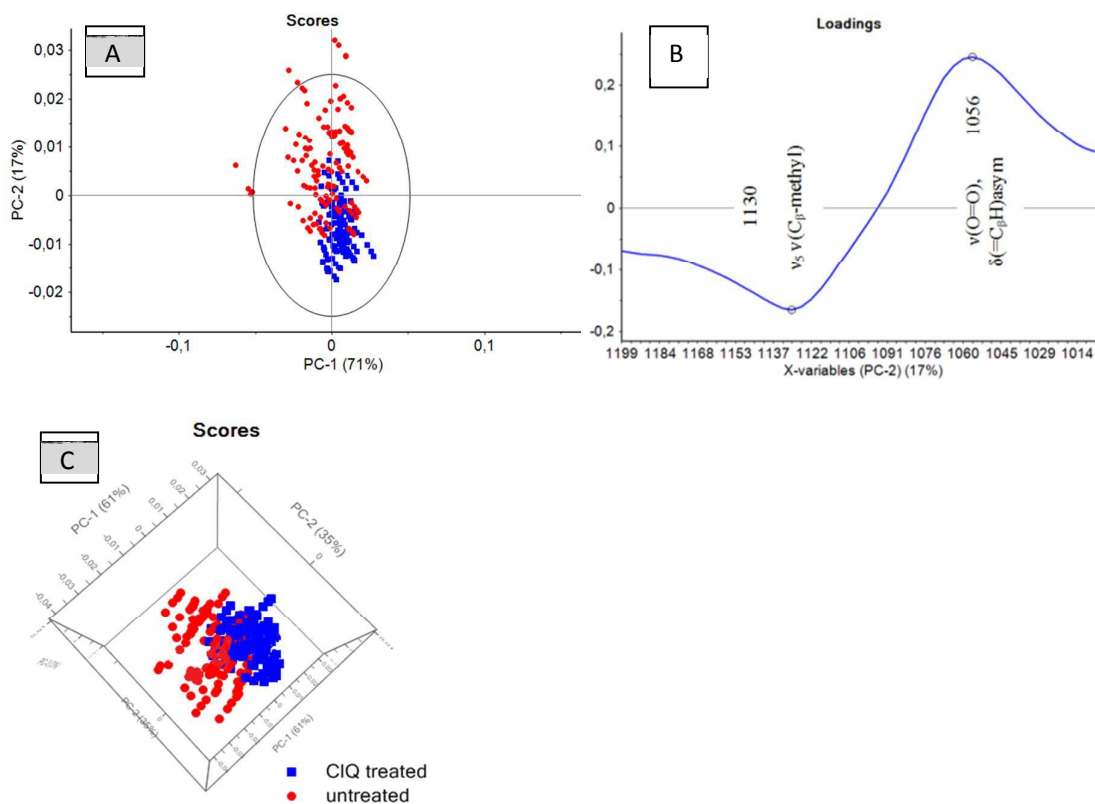
Fig. 4 A) PCA scores plot for PC-1 vs. PC-2 of untreated (red dots) and CQ-treated iRBCs (blue dots) based on second-derivative ATR-FTIR spectra in the 1200 - 1000 cm^{-1} region B) corresponding PCA-2 loadings plot C) 3D scores plot for PC-1 vs. PC-2 vs. PC-3.

The positive loadings at 1056 cm^{-1} ν(O=O) are correlated with negative scores along PC2 which indicates predominance of oxygenated hemoglobin in the CQ-treated iRBCs (Fig. 4). This is in the agreement with the results obtained by Raman spectroscopy, where bands ν_4(1379 cm^{-1}), ν_{11}(1550 cm^{-1}), ν_{19}(1604 cm^{-1}) and ν_{37}(1589 cm^{-1}) confirm the hemoglobin oxygenation state (see below). The separation of data along PC2 is the result of differences in the intensity of the ν_5 ν(C$_\beta$-C) band at 1130 cm^{-1} which is less intensive in CQ-treated iRBCs.
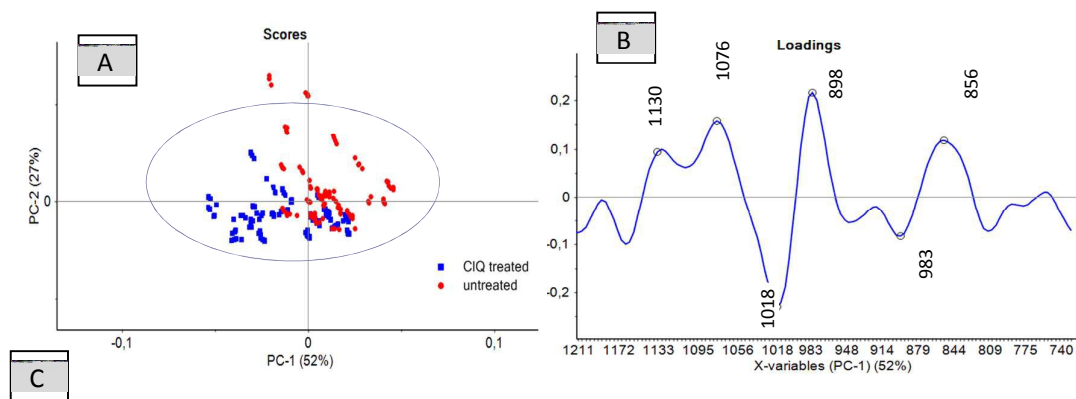
Fig. 5 Principal components analysis A) scores plot for PC-1 vs. PC-2 on second derivative ATR- FTIR spectra for the 1215 - 730 cm^{-1} region B) corresponding PCA-1 loadings with C) a table of band assignment for these loadings.

PC1 loadings [cm^{-1}]	Band assignments
856	v_{32} v(Pyr. def)$_{asym}$ [26]
898	DNA marker bands [17] ; CH from
983	RNA ribose chain [18]
1018	C-O from carbohydrates [18]
1076	phosphodiester groups from nucleic acids and
1130	phospholipids acyl chain C-C stretching [19, 20]

The strong negative loadings are indicative of carbohydrate bands prominent for the untreated iRBCs (Fig. 5C). Hence, it can be concluded that untreated iRBCs contain larger amounts of carbohydrate. This observation confirms the hypothesis of energy fabrication by *P. falciparum* through glycolysis during its intraerytrocytic development [21]. Glucose consumption is 50-100 times greater in iRBCs compared to RBCs. Most of the glucose is metabolized to lactic acid [22].

The large PC1 positive loadings in the 1215 - 730 cm^{-1} range may be attributed to the parasite-associated RNA vibrations and show a correlation with CQ-treated iRBCs. *P. falciparum* produce functionally different ribosomes in different developmental stages. After invasion, ribosomes begin to proliferate with membrane-associated protein synthesis. The thicker periphery of early stage parasites (ring-stage *P. falciparum*) contains the nucleus and the majority of the ribosomes. CQ is known to bind several forms of nucleic acids including DNA, tRNA, polydeoxyribonucleotides or polyribonucleotides. CQ also inhibits reactions

involving nucleic acid, where electrostatic interactions are known to play a key role [17]. It is not clear whether the observed perturbations to RNA, carbohydrates, lipids and hemoglobin metabolism indicate direct targeting of these pathways by CQ, or whether these are secondary biochemical responses. Nevertheless, this unbiased spectroscopic profiling of CQ action reveals a number of pathways that are involved in the mechanism of quinoline-induced *P. falciparum* death.

3.2 Raman microspectroscopy

Raman spectra extracted from Raman images of untreated and CQ-treated iRBCs. KCA clustering revealed three distinct root clusters associated with background, hemoglobin and hemozoin (Fig. 6). Spectra were extracted from the red cluster associated with hemoglobin and analysed separately to those extracted from the green cluster associated with hemozoin.
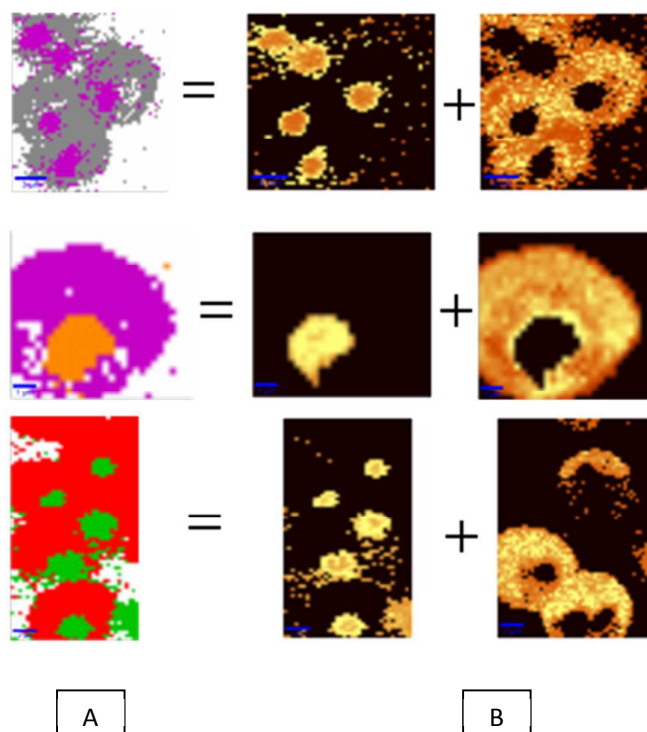
Fig. 6 The Raman distribution images of the *P. falciparum* - iRBCs obtained by using K Means Cluster Analysis for random chosen cells A) cluster analysis showing two root clusters (hemoglobin and hemozoin) B) Raman distribution images of the corresponding images (integration over $1670 - 1500$ cm^{-1} range).
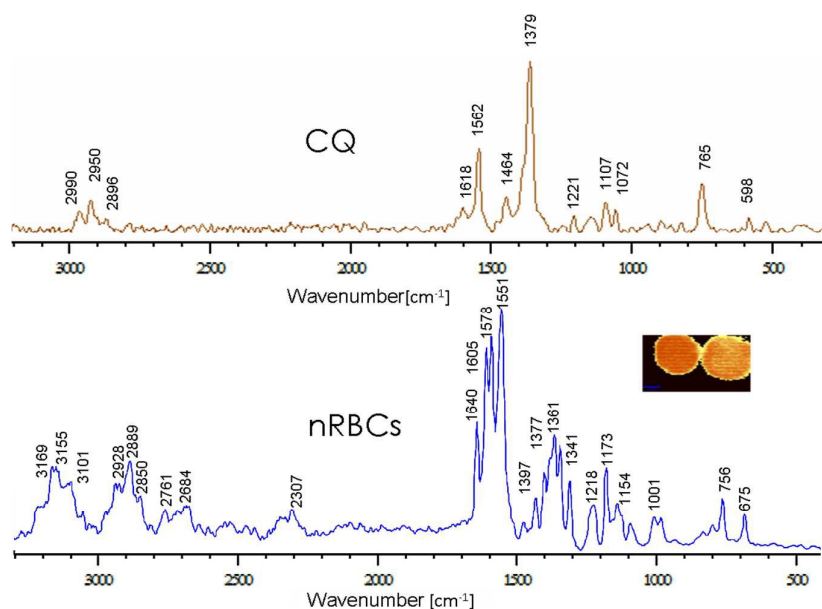
Fig. 7 Raman spectra of chloroquine (CQ) and non-infected red blood cells (nRBCs) using 532 nm excitation.
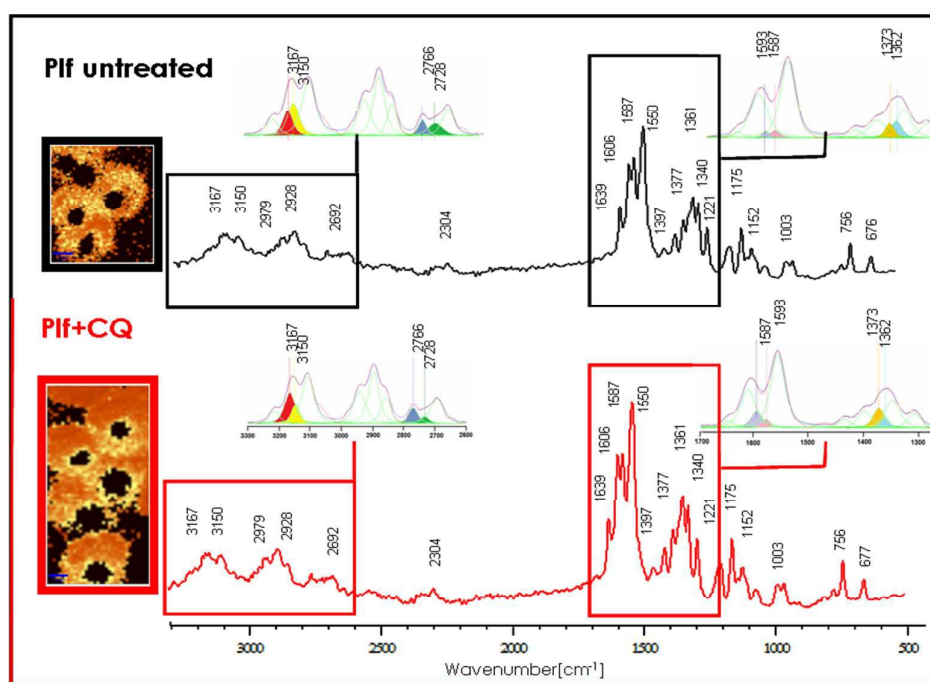
Fig. 8 Raman spectra of untreated (Plf untreated) and CQ-treated (Plf+CQ) from the hemoglobin region of *P. falciparum*- iRBCs using 532 nm excitation. The insets show curves fitted spectral ranges (left 3300-2600 cm^{-1}; right 1700-1300 cm^{-1}).
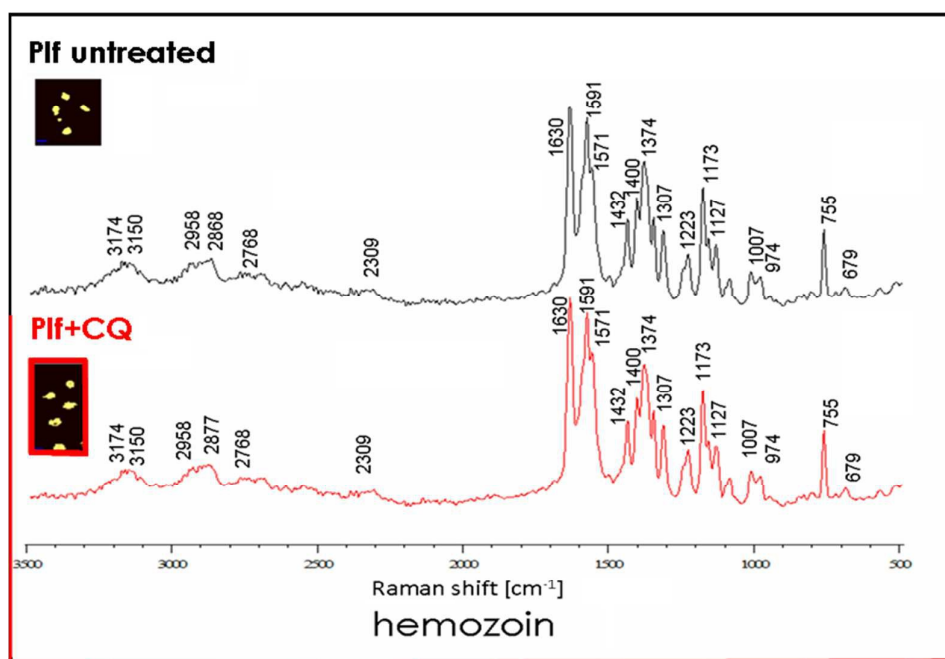
Fig. 9 Raman spectra of untreated (Plf untreated) and CQ-treated (Plf+CQ) from the hemozoin region of *P. falciparum*- iRBCs using 532 nm excitation.

Table 3. Observed wavenumbers and their assignments of non-infected red blood cells (nRBCs), untreated (Plf) and chloroquine-treated (Plf + CQ) *P. falciparum* - iRBCs using 532 nm excitation

Raman band positions [cm^{-1}]			Assignments [23,24,25,26,27]
nRBC	Plf	Plf + CQ	
3169	3174	3174	2 x ν_{37} (oxyHb)
3155	3149	3150	2 x ν_{37} (deoxyHb)
3101	3106	3106	2 x ν_{11}
2975	2979	2979	CH$_3$ asym. str.
2928	2928	2928	CH$_2$ asym. str. ; $\nu_{11 + 41}$
2889	2892	2892	CH$_2$ asym. str.
2850	2856	2856	CH$_2$ sym. str.
2761	2767	2767	2 x ν_4 (oxyHb)
2728	2726	2730	2 x ν_4 (deoxyHb)
2684	2682	2682	2 x ν_{41}
2307	2304	2304	2 x ν_{44}
1640	1639	1639	ν_{10} $\nu(C_\alpha C_m)_{asym}$
1605	1606	1606	ν_{19} $\nu(C_\alpha C_m)_{asym}$
1593	1594	1593	ν_{37} $\nu(C_\alpha C_m)_{asym}$ (deoxyHb)

14

1588	1578	1578	$\nu_{37}\,\nu(C_\alpha C_m)_{asym}$ (oxyHb)
1551	1550	1550	$\nu_{11}\,\nu(C_\beta C_\beta)$
1397	1397	1397	$\nu_{20}\,\nu$ (pyr quater-ring)
1377	1377	1377	$\nu_4\,\nu$(pyr half-ring)$_{sym}$ (oxyHb)
1361	1361	1361	$\nu_4\,\nu$(pyr half-ring)$_{sym}$ (deoxyHb)
1341	1340	1340	$\nu_{41}\,\nu$(pyr half-ring)$_{sym}$
1303	1306	1307	$\nu_{21}\,\delta(C_mH)$
1218	1221	1221	ν_{13} or ν_{42} $\delta(C_mH)$
1173	1175	1175	$\nu_{30}\,\nu$(pyr half-ring)$_{asym}$
1154	1152	1152	$\nu_{44}\,\nu$(pyr half-ring)$_{asym}$
1001	1003	1003	Phenylanaline
756	756	756	$\nu_{15}\,\nu$(pyr breathing)
675	676	677	$\nu_7\,\delta$(pyr deform)$_{sym}$

Table 4. Raman bands positions and their assignments for chloroquine using 532 nm excitation.

Raman band positions [cm^{-1}]	Assignments [28]
2990	C-H stretching in quinoline
2950	
2896	
1618	stretching mode in quinoline ring
1562	ν C=C in quinoline
1464	
1379	ν C=C and δ CH quinoline
1221	out of phase ring breathing and δ CH quinoline
1107	ν C=C and δ CH quinoline
1072	ν C=C quinoline
765	ring deformations and δ CH quinoline
598	δ C=C quinoline

Figure 7 shows Raman spectra recorded for CQ and non-infected RBCs (nRBCs). The band assignments are explained in Table 3 and 4. Raman spectra of untreated (Plf untreated) and CQ-treated (Plf+CQ) extracted from the haemoglobin region of iRBCs and their curve fitted spectral regions (inset) are shown in Figure 8 while the band assignments are shown in Table 3. Raman spectra of hemozoin did not change during our experiment (Fig. 9). This is not surprising as quantitative information is not possible under resonant conditions because of non-linear optical responses due to molecule orientation and excitonic effects [8].

Furthermore, because of the high confocality of the instrument (~1μm) not all hemozoin would be sampled in a given image plane.

In the high-wavenumber region (3200-2300 cm^{-1}) the first overtone modes of the porphyrin vibrations and CH_2 and also CH_3 groups can be observed. The fundamental marker band (v_4) has an overtone observed at 2761 cm^{-1}, which can be used as marker band for oxygenated RBCs (low spin, Fe^{3+}). Another significant overtone is from the v_{37} band for oxygenated hemoglobin, which is observed at 3169 cm^{-1}, while the corresponding band in deoxygenated hemoglobin appears at 3155 cm^{-1} [24]. In the 3100-2800 cm^{-1} range the acyl chain lipid bands dominate the spectrum. For untreated (Fig. 8) iRBCs a greater contribution of hemoglobin in the deoxygenated form was noted with bands at 2722 and 3150 cm^{-1}, which originate from the $2 \times v_4$ and $2 \times v_{37}$ overtones, respectively. The opposite situation can be observed for CQ treated cells with stronger bands at 2754 and 3175 cm^{-1} assigned to the oxygenated form of hemoglobin [24]. The $2 \times v_4$ integral intensity ratio from 2754 to 2722 cm^{-1} is equal to 2.42±0.34 and 0.38±0.11 for the oxygenated and deoxygenated state, respectively. The intensity ratio for the $2 \times v_{37}$, 3175 to 3150 cm^{-1} is equal to 2.15±0.49 and 0.68±0.04 for oxygenated and deoxygenated state, respectively. The above ratios can be treated as verification of the band assignments for the pyrrole ring and core size vibrations region in the fundamental region.

In the RBCs the core size and spin marker band region (1650-1500 cm^{-1}) is comprised of characteristic bands appearing at 1551-1550, 1588-1587, 1606-1605, 1640-1639 cm^{-1} assigned to v_{11}, v_{37}, v_{19} and v_{10}, respectively. v_{10} is a B_{1g} mode under D_{4h} symmetry and is particularly sensitive to porphyrin distortion. Translocation of the Fe ion out of the heme plane during oxygenation causes an increase of the intensity of this band. The v_{37} vibration intensity is sensitive to the oxygenated/deoxygenated state of iRBCs. The integrated intensity ratio of v_{37} of 1587 to 1575 cm^{-1} was equal to 2.41±0.20 and 0.63±0.06 for the oxygenated and deoxygenated state, respectively. The overtone region confirms this ratio calculation (Fig. 8, inset, left).

Bands in the pyrrole-ring stretching region (1400-1300 cm^{-1}) contain: v_{20} (1397 cm^{-1}), v_{41} (1341-1340 cm^{-1}) and the most intense band appears between 1377-1361 cm^{-1} and is assigned to the v_4 mode. For 532 nm excitation the v_4 bands appear at 1377 and 1361 cm^{-1} in the oxygenated and deoxygenated states, respectively.

The importance of ν_4 mode as a marker band of the oxygenated/deoxygenated state of heme molecules within RBCs was previously identified [25]. In this experiment the measurements were performed on single *cells* excited using a 532 nm laser line. It is worth noting that spectra recorded with a nearby excitation at 514.5 nm show two bands appearing at 1372 and 1357 cm^{-1} in the oxygenated state, whereas in the deoxygenated state a single band is observed at 1356 cm^{-1} [25]. The ν_4 band is the most intense band observed in the 488 and 514.5 nm spectra for both the oxygenated and deoxygenated states. At the longer wavelengths, 568 and 632.8 nm, the intensity of this band significantly reduces. This pattern can be observed in the spectra (Figs. 8 and 9) showing ν_4 to be somewhat reduced especially in the case of the ferric marker band at 1372 cm^{-1}. Analyzing the intensity relations of the corresponding bands within the complex pyrrole-ring stretching region can unravel information about the oxygenated/deoxygenated state. The integral intensity ratio of 1377 to 1361 cm^{-1} is equal to 2.43 ± 0.27 and 0.72 ± 0.08 for oxygenated and deoxygenated states, respectively (Fig. 8, inset, right). These results agree very well with the intensity ratio for band coming from ν_4 in the overtone region (Fig. 8, inset, left) and were duplicated in a second trial (see Electronic Supplementary Information).

In the low-wavenumber region (1200-500 cm^{-1}) bands are present at 1175-1173 cm^{-1} and 1154-1152 cm^{-1} assigned to ν_{30} and ν_{44} (ν(pyr half-ring)$_{asym}$), respectively. Other bands in this region, characteristic for oxygenated RBCs, are observed at 677-675 cm^{-1} (symmetric pyrrole deformation mode) and 756 cm^{-1} (pyrrole breathing mode) assigned to ν_7 and ν_{15}, respectively [25].

The Raman spectrum of CQ (Fig. 7) in the 3100-2800 cm^{-1} range shows CH stretching vibrations from the quinoline functional group. The intensity of the Raman bands between 1600-1000 cm^{-1} are assigned to quinoline C=C stretching and CH_2/CH_3 deformation vibrations. The low-wavenumber range is characterized by C=C deformation and quinoline ring deformation modes [28].

PCA was used in order to detect subtle changes in CQ-treated iRBCs and to check and confirm the observed intensity relationships for hemoglobin. The PCA scores plots (Fig. 10) show a general separation based on differences in the amount of oxygenated and deoxygenated hemoglobin between the CQ-treated and untreated iRBCs. The differences between the average spectra are confirmed by PCA analysis to the population of data. Because of the inherent biological variability, the clusters are not distinct and there is some

overlap. There were no significant differences in the spectra of hemozoin between CQ-treated and untreated iRBCs.
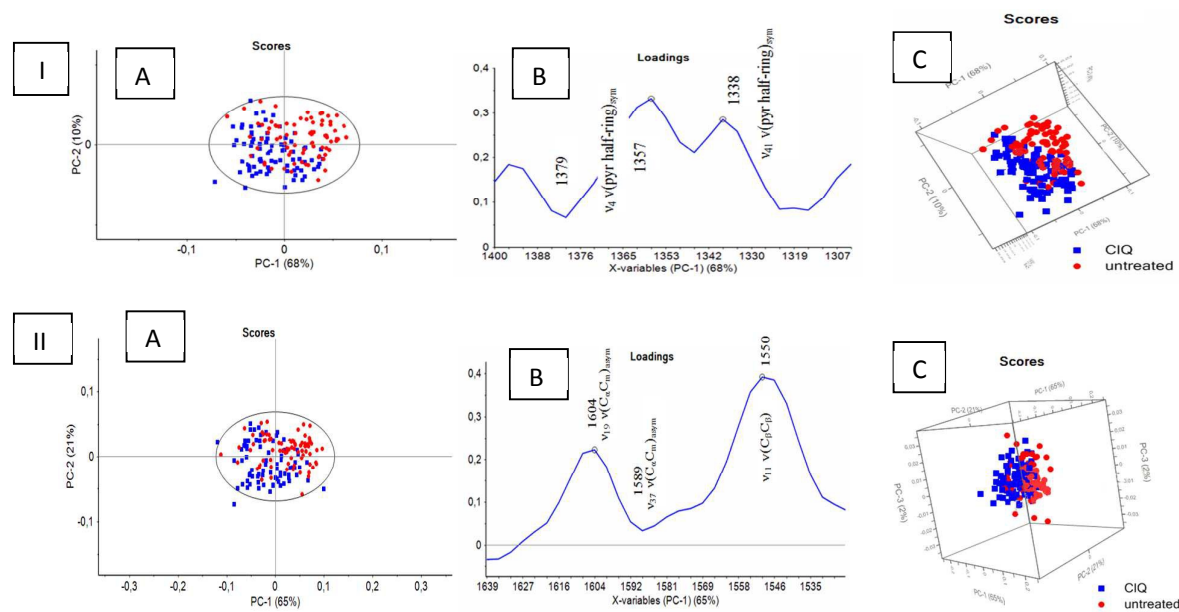
Fig. 10 Principal components analysis PC-1 vs. PC- 2 applied to Raman spectra, A) scores plot B) corresponding loadings plot and C) for PC-1 vs. PC-2 vs. PC-3, 3D scores plot, showing a general separation between CQ-treated (blue dots) and untreated (red dots) *P. falciparum* - iRBCs for I) 1400 - 1300 cm^{-1} and II) 1640 – 1520 cm^{-1} region using 532 nm excitation.

The PC1 loadings in the 1400 - 1300 cm^{-1} range (Fig. 10. I) show evidence of a high oxygenated hemoglobin concentration in the CQ-treated iRBCs as confirmed by the minima band at 1379 cm^{-1} which is assigned to v_4 [25]. This is characteristic of ferric heme, which is the oxidation state of the Fe ion when in the oxygenated state. Conversely a higher concentration of deoxygenated hemoglobin is observed in the untreated iRBCs as evidenced by the maxima band at 1357 cm^{-1}, which is typical for the oxidation state of a ferrous heme characteristic of deoxygenated hemoglobin. This shift is thought to reflect the electron population in porphyrin π^* orbitals. It follows that an increase of electron population in porphyrin π^* orbital weakens the bonds resulting in a shift towards lower wavenumber [25]. Hence the v_4 band position shifts in response to CQ treatment and may be an indicator of CQ effectiveness.

Other evidence indicative of an oxygenation-state change is marked by the appearance of v_{19} and v_{37} bands ($v(C_\alpha C_m)$ vibrations) at 1604 and 1589 cm^{-1}, respectively along with v_{11}

$\nu(C_\beta C_\beta)$ at 1550 cm^{-1}, sensitive to the nature of the hemoglobin peripheral substituents [14]. Positive loadings in the 1640 – 1520 cm^{-1} range (Fig. 10. II) show three principal bands 1550, 1589 and 1604 cm^{-1} assigned to ν_{11}, ν_{37} and ν_{19}, respectively. These bands are known marker bands for the high spin state of deoxygenated hemoglobin in the untreated iRBCs and are enhanced when 532 nm excitation is applied [25, 26].

4. Conclusions

The changes in the intensity of vibrational bands following CQ treatment indicate changes in the molecular environment of the cultured *P. falciparum* - iRBCs. ATR-FTIR and Raman microscopy provide complementary results. ATR-FTIR identified changes in proteins, lipids, nucleic acids and carbohydrates in response to CQ treatment, while Raman microspectroscopy can provide information about the oxygenation status of hemoglobin in CQ-treated iRBCs compared to untreated iRBCs under laboratory conditions. More work is required to determine the applicability of the Raman technique for monitoring oxygenated hemoglobin status in drug treated cells including setting up calibration standards to accurately determine oxyhemoglobin content at the single cell level.

The ATR-FTIR results show an increase in the CH stretching bands in the 3100 -2800 cm^{-1} region in CQ-treated iRBCs consistent with an increased abundance of saturated lipids. The drug addition caused changes in the secondary structure of proteins but these are difficult to interpret because of bound water and Mie scattering artifacts which can shift the amide I position. KCA and PCA methods were applied to discriminate untreated and CQ-treated iRBCs. This work provides contribution into understanding of the modes of action of antimalarial drugs on the single cell level and demonstrates how FTIR and Raman can provide ways to assess the impact of antimalarials on cellular biochemistry.

5. Acknowledgment

Electronic Supplementary Information (ESI) available.

6. References

[1] T. Harinasuta, P. Suntharasamai, C. Viravan, Chloroquine-resistant falciparum malaria in Thailand, *The Lancet*, 1965, 2 ,657–60

[2] WHO. World Malaria Report 2011, Geneva, WHO, 2011

[3] A.F.G. Slater, Chloroquine: mechanism of drug action and resistance in *Plasmodium falciparum*, *Pharmacol. Ther.*, 1993, 57, 203-35

[4] P.G. Bray, S.R. Hawley, M. Mungthin, S.A. Ward, Physicochemical properties correlated with drug resistance and reversal of drug resistance in *Plasmodium falciparum*, *Mol Pharmacol.*, 1996, 50, 1559-66

[5] D.J. Krogstad, P,H. Schlesinger, A perspective on antimalarial action: effects of weak bases on *Plasmodium falciparum*, *Biochemical Pharmacology*, 1986, 35, 547-52

[6] P.G. Bray, O. Janneh, K. J. Raynes, M. Mungthin, H. Ginsburg, S. A. Ward, Cellular Uptake of Chloroquine Is Dependent on Binding to Ferriprotoporphyrin IX and Is Independent of NHE Activity in *Plasmodium falciparum*, *J. Cell Biol.*, 1999, 145

[7] A.B. Singh Sidhu, D. Verdier-Pinard, D. A. Fidock, Chloroquine Resistance in *Plasmodium falciparum* Malaria Parasites Conferred by pfcrt Mutations, *Science*, 2002, 298, 210-213

[8] B.R. Wood, S.J. Langford, B.M. Cooke, J. Lim, F.K. Glenister, M. Duriska, J.K. Unthank, D. McNaughton, Resonance Raman spectroscopy reveals new insight into the electronic structure of -hematin and malaria pigment, Journal of the American Chemical Society, 2004, 126, 9233-9239

[9] W. Trager, J. B. Jensen, Human malaria parasites in continuous culture, *Science*, 1976, 193, 673-675

[10] Asghari-Khiavi, A.I. Mechler, K.R. Bambery, D. McNaughton, B.R. Wood, A resonance Raman spectroscopic investigation into the effects of fixation and dehydration on heme environment of hemoglobin, Journal Of Raman Spectroscopy, 2009, 40, 1668-1674

[11] M. Szczerbowska-Boruchowska, P. Dumas, M. Zofia Kastyak, J. Chwiej, M. Lankosz, D. Adamek, A. Krygowska-Wajs, Biomolecular investigation of human substantia nigra in Parkinson's disease by synchrotron radiation Fourier transform infrared microspectroscopy, *Arch. Biochem. Biophys,* 2007, 459, 241–248

[12] G. Socrates, Infrared characteristic group frequencies, John Wiley& Sons, Ltd., Chichester, 1980

[13] T. J. Dines, L. D. MacGregor, C. H. Rochester, IR Spectroscopic Investigation of the Interaction of Quinoline with Acidic Sites on Oxide Surfaces, *Langmuir,* 2002, 18, 2300-2308

[14] K. Nakamoto, Infrared and Raman spectra of inorganic and coordination compounds, Part B, John Wiley& Sons, Inc., New York, 1997

[15] C. A. Clavijo, C. A. Mora, E. Winograd, Identification of Novel Membrane Structures in *Plasmodium falciparum* Infected Erythrocytes, *Mem Inst Oswaldo Cruz*, 1998, 93, 115-120

[16] L.L. Hsiao, R. J. Howard, M. Aikawa, T. F. Taraschi, Modification of host cell membrane lipid composition by the intra-erythrocytic human malaria parasite *Plasmodium falciparum*, *Biochem. J.*, 1991, 274, 121-13

[17] R. Roskoski, S. R. Jaskunas, Chloroquine and primaquine inhibition of rat liver cell-free polynucleotide-dependent polypeptide synthesis, *Biochemical Pharmacology*, 1972, 21, 391-399

[18] B. R. Wood, B. Tait, D. McNaughton, Fourier Transform Infrared Spectroscopy as a Method for Monitoring the Molecular Dynamics of Lymphocyte Activation, *Appl. Spectrosc.*, 2000, 54, 353–359

[19] M. Tsuboi, Applied Spectroscopy Reviews, ed. M. Dekker, John Wiley and Sons, New York, 1970, Vol. III, 45-90.

[20] T. Shimanouchi, M. Tsuboi, Y. Kyogoku, Infrared Spectra of Nucleic Acids and Related Compounds, Advances in Chemical Physics, ed. J. Duchesne, Interscience, London, 1964, Vol. VII, 435-468

[21] M.J. Gardner, N. Hall, E. Fung, O. White, M. Berriman, R.W. Hyman, J.M. Carlton, A. Pain, K.E. Nelson, S. Bowman, I.T. Paulsen et.al., Genome sequence of the human malaria parasite Plasmodium falciparum, Nature, 2002, 419, 498–511

[22] I. W. Sherman, L. Tanigoshi, Glucose transport in the malarial (Plasmodium lophurae) infected erythrocyte, J. Protozool., 1974, 21, 603-607

[23] G.T. Webster, L. Tilley, S. Deed, D. McNaughton, B. R. Wood, Resonance Raman spectroscopy can detect structural changes in haemozoin (malaria pigment) following incubation with chloroquine in infected erythrocytes, FEBS Letters, 2008, 582, 1087–1092

[24] K. M. Marzec, D. Perez-Guaita, M. de Veij, D. McNaughton, M. Barańska, M. W. A. Dixon, L. Tilley, B. R. Wood, Red blood cells polarize green laser light revealing hemoglobin's enhanced non-fundamental Raman modes, Chem Phys Chem 2014, 15, 1-7

[25] B.R. Wood, D. McNaughton, Raman excitation wavelength investigation of single red blood cells in vivo, J. Raman Spectrosc., 2002, 33, 517-523

[26] M. Abe, T. Kitagawa, Y. Kyogoku, Resonance Raman spectra of octaethylporphyrinato-Ni(II) and meso-deuterate and 15N substituted derivatives. II, J. Chem. Phys, 1978, 69, 4526 – 4534

[27] A. Wesełucha-Birczyńska, M. Kozicki, J. Czepiel, M. Łabanowska, P. Nowak, G. Kowalczyk, M. Kurdziel, M. Birczyńska, G. Biesiada, T. Mach, A. Garlicki, Human

erythrocytes analyzed by generalized 2D Raman correlation spectroscopy, J. Mol. Struct., 2014, 1069, 305–312

[28] T. Frosch, M. Schmitt, G. Bringmann, W. Kiefer, J. Popp, Structural Analysis of the Anti-Malaria Active Agent Chloroquine under Physiological Conditions, J. Phys. Chem. B, 2007, 111, 1815-1822